Appl. Phys. B 77, 607–612 (2003)
DOI: 10.1007/s00340-003-1327-z

Applied Physics B
Lasers and Optics

J. HERREROS-CEDRÉS
C. HERNÁNDEZ-RODRÍGUEZ✉
B. GONZÁLEZ-DÍAZ
R. GUERRERO-LEMUS

Temperature-dependent optical anisotropy of L-arginine phosphate single crystal

Departamento de Física Básica, Facultad de Física, Universidad de La Laguna, Avda. Francisco Sánchez s/n°, 38206 La Laguna, Tenerife, Spain

Received: 21 April 2003/Revised version: 25 July 2003
Published online: 29 October 2003 •

ABSTRACT The optical anisotropy at different temperatures (birefringence, complete optical gyration tensor, and optical indicatrix rotation) for a monoclinic crystal of L-arginine phosphate has been determined by using the high-accuracy universal polarimeter (HAUP) method at a wavelength of 632.8 nm. The thermal variation coefficients of the birefringence along the (010), (101), (100), and (−201) planes were found to be $-25.9\times10^{-6}\,\mathrm{K}^{-1}$, $11.1\times10^{-6}\,\mathrm{K}^{-1}$, $6.4\times10^{-6}\,\mathrm{K}^{-1}$, and $-10.7\times10^{-6}\,\mathrm{K}^{-1}$, respectively. The tensor components in terms of rotatory power were found to be $\varrho_{11}=-6.6°/\mathrm{mm}$, $\varrho_{22}=19°/\mathrm{mm}^{-1}$, $\varrho_{33}=49.7°/\mathrm{mm}$, and $\varrho_{13}=-43.7°/\mathrm{mm}$ at room temperature.

PACS 78.20.Ek; 78.20.Fm; 42.70.Jk; 07.60.Fs

1 Introduction

L-arginine phosphate monohydrate (LAP) is one of the essential amino acids widely distributed in biological substances. It occurs mostly as a constituent of proteins, especially protamine, but in some materials, such as seeds, it occurs as a free amino acid [1]. We have set out to investigate its gyro-optical properties because these studies are necessary for a deeper understanding of the biological functions of various proteins. In addition, measurements of optical anisotropy in monoclinic crystals are complicated by the long-standing difficulty of measuring the complete gyration tensor in this kind of crystal, for which only a few measurements are known [2–4].

LAP is a promising nonlinear organic crystal, whose properties were first reported by Xu et al. [5]. It can be phase matched with all nonlinear processes for which potassium dihydrogen orthophosphate (KDP) can be phase matched. It has been found that LAP is three times more nonlinear than KDP and that its damage threshold is also two to three times higher than that of KDP [6–8].

The thermal expansion of LAP crystals is highly anisotropic and the dielectric constants and resistivity exhibit a temperature dependence that is similar to that of an ionic crystal [9]. There are no phase transitions between 283 K and the temperature at which chemical decomposition sets in, around 403 K [6]. We have studied the optical anisotropy at temperatures up to 359 K because the crystal begins to soften at temperatures above 373 K, and then liquefies in the range 393–413 K [10].

Large LAP crystals of high optical quality can easily be grown from a water solution, being less hygroscopic than KDP crystals and having a wide transparency range [6, 11]. The structure at room temperature was first solved by Aoki et al. [1] and the accuracy of the structure was later improved by Saenger and Wagner [12]. The LAP formula unit can be written as $(H_2N)_2^+CNH(CH_2)_3CH(NH_3^+)COO^-\cdot H_2PO_4^-\cdot H_2O$. The crystal is monoclinic, and of point group 2 and space group $P2_1$, with two formula units per cell [1, 6, 12]. The cell dimensions are $a=1.085$ nm, $b=0.791$ nm, $c=0.732$ nm, and $\beta=98°$ at 298 K.

This article is organized as follows: in Sect. 2 we describe the different reference systems used and the expression for the gyration tensor of LAP. The equations of the high-accuracy universal polarimeter (HAUP) method and the experimental results are presented in Sect. 3. This section is further divided into two parts to discuss the results for the birefringence and gyration tensor of LAP. Conclusions are given in Sect. 4.

2 Optical nature

In order to study the different optical properties of the biaxial LAP crystal, it is convenient to define an orthogonal system (e_1, e_2, e_3), because the crystallographic axes (a, b, c) are not mutually orthogonal in the monoclinic system. Our system was chosen according to the international convention for specifying the physical reference system as a basis of tensors [2, 10]. Thus, the e_2 and e_3 axes were taken parallel to the monoclinic b and c axes, respectively, and $e_1=b\times c$, as shown in Fig. 1. The principal axes of the indicatrix were defined as (x, y, z) and the associated refractive indices as $n_x<n_y<n_z$.

For monoclinic crystals, the crystallographic symmetry requires that the twofold crystallographic axis (b) also be a principal axis of the indicatrix. Eimerl et al. defined the orientation of the dielectric axes (x, y, z) and their sense [6, 13], with the y axis parallel to the crystallographic b axis and the z axis making an angle of 35° with the c axis in the plane (ac). The optic axes of the biaxial crystal lie in

✉ Fax: +34-922/318-228, E-mail: chdezr@ull.es

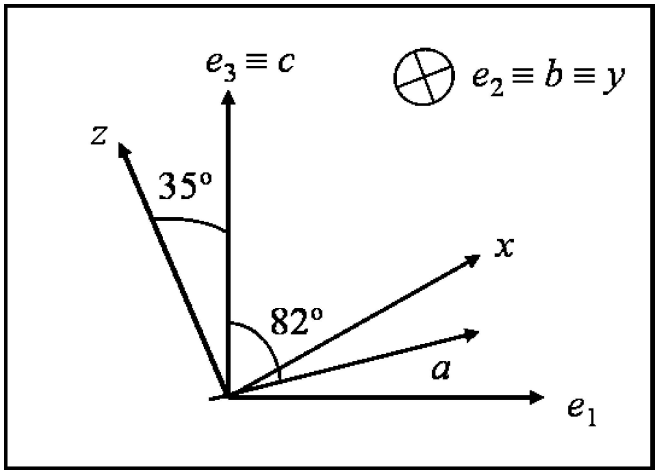

FIGURE 1 Relation between the reference axes (e_1, e_2, e_3), the crystallographic axes (a, b, c), and the principal axes (x, y, z) of the indicatrix of LAP. The b axis (parallel to e_2 and y) lies perpendicular to the plane of the drawing

the (xz) plane, perpendicular to y. The relations between the reference axes (e_1, e_2, e_3), the crystallographic axes (a, b, c), and the principal axes (x, y, z) of the indicatrix are shown in Fig. 1.

The components of the gyration tensor referred to the reference axes are expressed by the matrix [14]

$$\begin{bmatrix} g_{11} & 0 & g_{13} \\ 0 & g_{22} & 0 \\ g_{13} & 0 & g_{33} \end{bmatrix}. \tag{1}$$

In order to determine the gyration tensor components, four different samples with Miller indices (010), (100), (101), and (−201), numbered as 1, 2, 3, 4, respectively, were studied. These crystals, supplied by Molecular Technology GmbH, were of very good optical quality (transparency and homogeneity, with well-polished faces). The plane orientation was checked with a polarization microscope, observing in conoscopic illumination.

3 Haup experiments

The measurements were carried out with the HAUP setup [15, 16] designed in our laboratory [17], from room temperature to 359 K in steps of 2 K with an accuracy of ±0.05 K. The light source was an He–Ne laser with a wavelength of 632.8 nm.

In the HAUP method, the sample is placed between nearly crossed polarizers. Under conditions of small azimuths Θ of the polarizer with respect to the fast axis of the sample, the relative intensity of the transmitted light through the analyzer, Γ, is given by

$$\Gamma = A + B\Theta + C(\Theta^2 + \Theta Y) + DY + Y^2, \tag{2}$$

where Y is the analyzer angle with respect to the position of the crossed polarizers. A, B, C, and D are coefficients (HAUP coefficients) related to the systematic errors of the device and the optical properties of the material. For all measurements, both the sample and analyzer are rotated around the minimum intensity positions (HAUP region). The set of intensity values allows the HAUP coefficients to be obtained by least-squares fitting [18]. The fitted coefficients that allow the birefringence, optical activity, and rotation of optical indicatrix to be obtained simultaneously are given by

$$C = 4\sin^2(\Delta/2), \tag{3}$$

$$\Theta_0 = -\frac{B}{2C} = -\frac{1}{2}(p+q)\cot\left(\frac{\Delta}{2}\right) + \frac{\delta Y}{2} + \Psi, \tag{4}$$

$$D' = D - (B/2) = (p-q-2k)\sin\Delta + 2\delta Y\cos^2(\Delta/2), \tag{5}$$

where $\Delta = [\delta(1+2k)]^{1/2}$ is the phase difference that the two elliptically polarized orthogonal components of the light beam suffer in their propagation through the crystal with different velocities, δ being the delay due to the birefringence and k the common ellipticity of the polarization ellipses. p and q are the residual ellipticities of the polarizer and analyzer, respectively, and δY an error in the determination of the position of the crossed polarizers [19]. In (4), Θ_0 represents physically the angle of minimal transmission and Ψ is the rotation of the optical indicatrix with the temperature or wavelength if spectral dispersion takes place.

3.1 *Temperature-dependent birefringence of LAP*

If the incident light is perpendicular to the face (010), the birefringence $\Delta n_{(010)} = \Delta n_y = n_z - n_x$ can be measured. For the rest of the specimens, the birefringence can be expressed in terms of $\Delta n_x = n_z - n_y$ and $\Delta n_z = n_y - n_x$ in the following way. Taking one sample, no. 4, for instance, the birefringence for this plane can be written as

$$\Delta n_{(-201)} = n_y - n, \tag{6}$$

where n is one of the principal refractive indices in the direction of the wave normal $\boldsymbol{s}$. From the dielectric impermeability normal to the $\boldsymbol{s}$ direction, n is expressed as

$$\frac{\sin^2\theta}{n_x^2} + \frac{\cos^2\theta}{n_z^2} = \frac{1}{n^2}, \tag{7}$$

where θ is the angle made by $\boldsymbol{s}$ and the x axis in the (010) plane, derived through geometric relations ($\theta \approx 68°$ for specimen no. 4, from lattice constants a and c).

In the case of our samples, the n refractive index could be written as (see the Appendix)

$$n \cong n_x\sin^2\theta + n_z\cos^2\theta, \tag{8}$$

the birefringence for the (−201) plane being

$$\Delta n_{(-201)} = n_y - n = \Delta n_z\sin^2\theta - \Delta n_x\cos^2\theta. \tag{9}$$

In the range of studied temperatures, the birefringence can be written as

$$\Delta n = \Delta n(T_\mathrm{i}) + \frac{\mathrm{d}\Delta n}{\mathrm{d}T}(T - T_\mathrm{i}), \tag{10}$$

with T_i being the initial temperature. The thermal variation coefficient of the birefringence, $\mathrm{d}\Delta n/\mathrm{d}T$, can be obtained from the experimental C values as

$$\frac{\mathrm{d}\Delta n}{\mathrm{d}T} = \frac{\lambda}{2\pi d}\left(\frac{\mathrm{d}\Delta}{\mathrm{d}T}\right), \tag{11}$$

d being the thickness of the specimen and λ the free-space wavelength.

Figure 2 shows the temperature dependence of the C coefficient for specimen no. 4, in two HAUP experiments for two consecutive extinction directions of the sample (see Sect. 3.2), where the high accuracy in the reproducibility of the measurements can be seen. The solid lines represent the best fits to (3) considering that the delay Δ has a linear dependence on temperature. There is a slight displacement of the C curve due to the fact that the plane-parallel plate is not perfectly perpendicular to the incident beam. In this case, the change of phase experienced by the transmitted light is given by [20]

$$\Delta(\theta_i) = \Delta(1 + \sin^2\theta_i/2\bar{n}^2), \tag{12}$$

where θ_i is the incidence angle and Δ is the change of phase at normal incidence. By introducing the delay Δ obtained from the fitting of the two curves of Fig. 2 in the last equation, a difference of $(\theta_{i(0°)} - \theta_{i(90°)}) = 3°$ in the incidence angle was found for the two sets of measurements in the two positions of the sample. This deviation in the incident direction of propagation was considered for further calculations.

The same treatment could be applied to the other specimens. The number, index of the surface perpendicular to the light beam, birefringence, and thickness of each specimen are tabulated in Table 1. It is clear that from the experimental birefringence values of two samples, nos. 2 and 4, for example, one can obtain theoretically the values for the other two planes. Results for the birefringence as a function of the temperature are represented in Fig. 3. In spite of the slight differences between the values of the theoretical and experimental birefringence of specimen nos. 1 and 3, the thermal dependence is almost the same, confirming the validity of the approximation made in (9). It can be seen that the birefringence varies linearly with temperature in the considered temperature range. From the adjustment carried out, the thermal variation coefficient for the birefringence can be extracted and is presented in Table 2 for each sample.

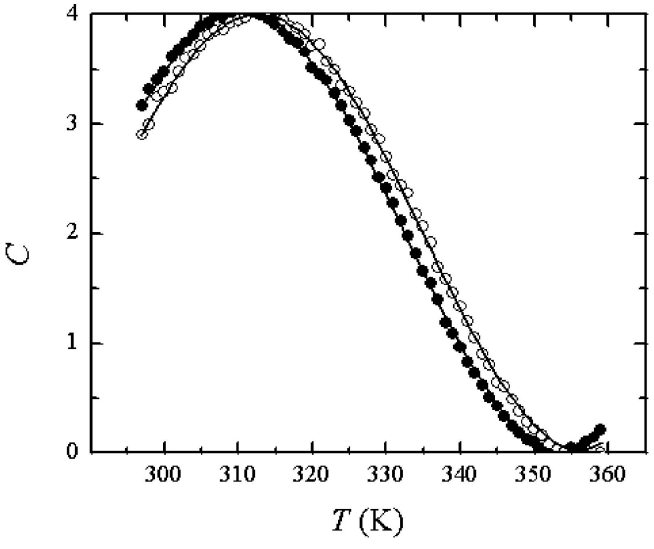

FIGURE 2 Temperature dependence of parameter C for the (-201) plane of LAP. *Open* and *filled circles* correspond to the two measurements for two consecutive extinction directions of the sample. The *solid lines* represent the fit to (3).

Sample no.	Surface planes	Thickness (mm)	Birefringence (Δn)[a]
1	(010)	0.479	Δn_y
2	(100)	0.719	$0.329\Delta n_z - 0.671\Delta n_x$
3	(101)	0.563	$0.197\Delta n_z - 0.803\Delta n_x$
4	(-201)	0.671	$0.865\Delta n_z - 0.135\Delta n_x$

[a] $\Delta n_x = n_z - n_y$, $\Delta n_y = n_z - n_x$, and $\Delta n_z = n_y - n_x$.

TABLE 1 Data for the specimens used

In the method proposed above, it has been supposed that the θ angle made by the direction of the wave normal $\boldsymbol{s}$ and one of the principal dielectric axes remains constant in the considered temperature range. However, if dispersion of the axes [21] occurs, this angle will vary with the temperature. To check whether the studied samples show this effect, the optical indicatrix rotation (Ψ) was considered. Ψ can be obtained through the angle of minimal transmission Θ_0 (see (4)). Only variations in these angles have physical meaning due to

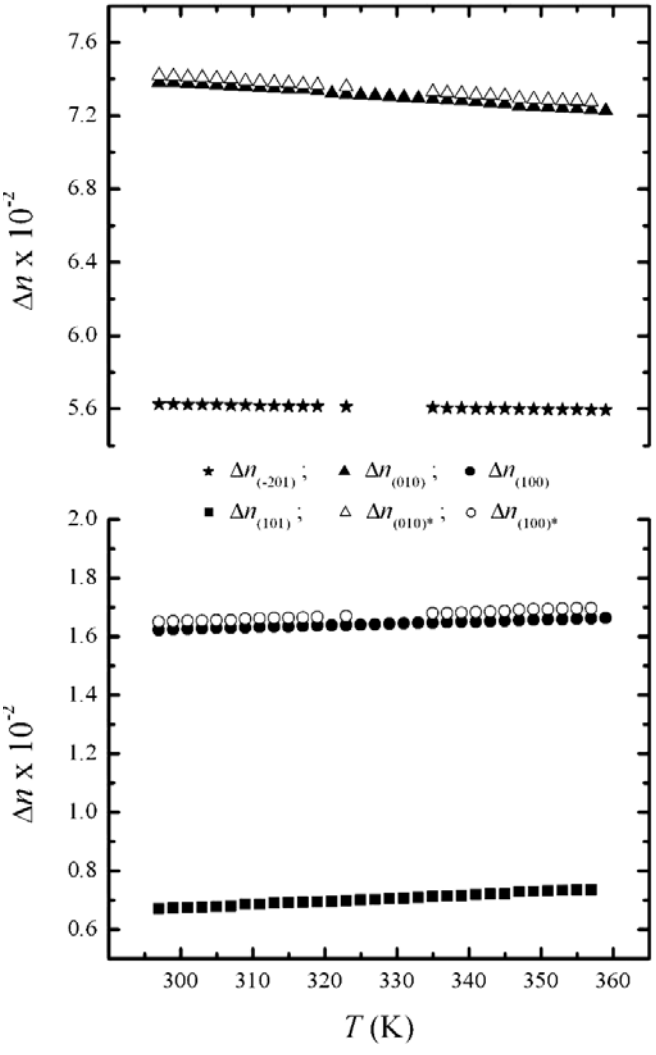

FIGURE 3 Temperature dependence of the mean birefringence. *Filled triangles*, *circles*, *squares*, and *stars* represent the experimental birefringence for the (010), (100), (101), and (-201) planes of LAP, respectively. *Open triangles* and *circles* correspond to the values obtained theoretically for the (010) and (100) planes, respectively

i	$(010) \equiv y$	(100)	(101)	(-201)	x	z
$\mathrm{d}(\Delta n_i)/\mathrm{d}T$	-25.9 ± 0.3	6.4 ± 0.2	11.1 ± 0.3	-10.7 ± 0.6	-16.9 ± 0.7[a]	-15 ± 2[a]
$\times 10 \times 10^{-6}$ (K^{-1})	-32 ± 3[a]		10.6 ± 0.9[a]			

[a] Calculated theoretically from (100) and (-201) planes.

TABLE 2 Thermal variation coefficient of the birefringence

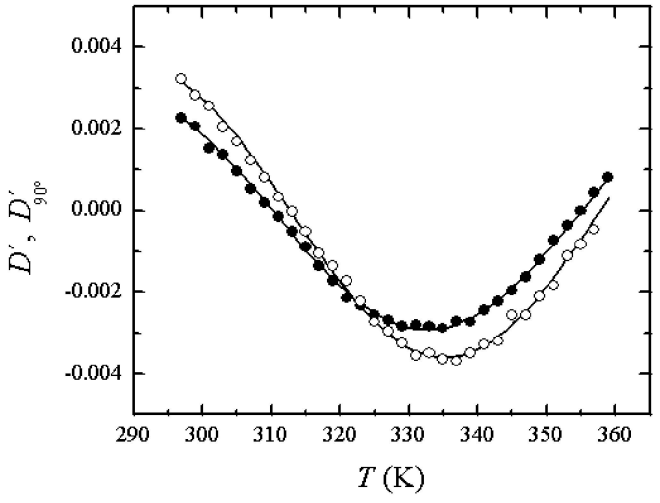

FIGURE 4 Dependence on the temperature of the parameters D' and $D'_{90°}$ obtained in two consecutive extinction directions of the (-201) plane of LAP. The *solid lines* represent the best fits to (5) and (13)

the fact that both Θ_0 and Ψ are referred to the origin of angles of the experimental setup, which is arbitrary. Figure 4 shows the variation with the temperature of the Θ_0 angle, in which it is appreciably larger in the sample with Miller indices (010) than in specimen nos. 2, 3, and 4. The variations with the temperature can be due to parasitic contributions through the function of (4), and therefore, the rotation of the optical indicatrix is nil. For sample no. 1, the Θ_0 angle seems to be larger, probably because around a temperature of 342 K the phase difference is $\Delta \cong 2n\pi$ (n integer), reaching the cotan$(\Delta/2)$ singularity in (4). The HAUP method has these disadvantages but, generally, the conflicting points may be ignored [22]. Thus, for LAP crystals, in the considered temperature range in which there are no phase transitions, rotation of the dielectric axes is absent, θ remains constant, and no errors are introduced in the estimation of the thermal variation coefficient of the birefringence.

3.2 *Determination of the gyration tensor components*

In order to determine the temperature dependence of the components of the gyration tensor, we should obtain the values of the ellipticity k for each temperature through (5). However, it is necessary first to eliminate the systematic errors $\gamma = p - q$ and δY. Following Moxon and Renshaw [18], the measurements were carried out for two consecutive extinction directions of the sample. The difference between the two sets of measurements is a change of sign in the delay Δ and the ellipticity k. Thus, the D' HAUP coefficient for the second set of measurements can be written as

$$D'_{90°} = -(\gamma_{90°} + 2k)\sin\Delta + 2\delta Y_{90°}\cos^2(\Delta/2), \tag{13}$$

bearing in mind the sign of k and Δ. The temperature dependencies of D' and $D'_{90°}$ of specimen no. 4 are represented in Fig. 5. Fitting this curves to (5) and (13), respectively, using γ, $\gamma_{90°}$, k, δY, and $\delta Y_{90°}$ as adjustment parameters, one can extract the value of the ellipticity k, taking into account that $|\gamma - \gamma_{90°}| \ll |4k|$. The values for the absolute ellipticities are shown in Table 3.

Finally, once the ellipticity k and the birefringence Δn have been obtained, the gyration along the beam direction can be derived from the relationship that ties the magnitudes above with G when the optical axes are far from the incident light beam:

$$G = 2k\bar{n}\Delta n, \tag{14}$$

where $\bar{n}$ is an effective refractive index of the sample.

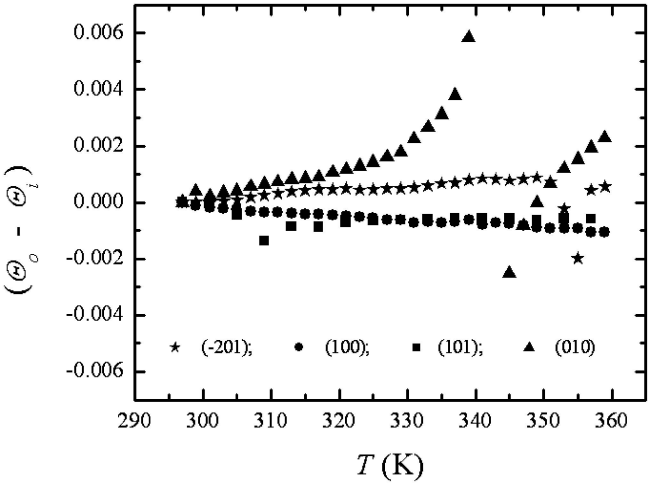

FIGURE 5 Temperature dependence of the angle of minimal transmission of LAP. *Triangles*, *circles*, *stars*, and *squares* correspond to the extinction angle for the (010), (100), (-201), and (101) planes, respectively

Sample no.	Surface planes	$\lvert k\rvert \times 10^{-4}$	(φ/d) (°/mm)	G
1	(010)	4.7 ± 0.4	19(2)	g_{22}
2	(100)	7.1 ± 0.2	$-6.6(3)$	g_{11}
3	(101)	0.2 ± 0.1	$-0.07(4)$	$0.230g_{11} + 0.770g_{33} + 0.842g_{13}$
4	(-201)	15.9 ± 0.1	50.7(5)	$0.696g_{11} + 0.304g_{33} - 0.920g_{13}$

TABLE 3 Absolute ellipticities, optical rotatory power at room temperature, and gyration magnitude as a function of the gyration tensor components, for the specimens used

The components of the gyration tensor (g_{ij}) can be obtained through [14]

$$G = s_i s_j g_{ij}, \qquad i,j = 1, 2, 3. \tag{15}$$

Here, s_i and s_j are the direction cosines of the normal wave $\boldsymbol{s}$ with respect to the reference axes (e_1, e_2, e_3). For the LAP crystal, (15) is reduced to

$$G = g_{11}\cos^2\alpha_1 + g_{22}\cos^2\alpha_2 + g_{33}\cos^2\alpha_3 + 2g_{13}\cos\alpha_1\cos\alpha_3. \tag{16}$$

The values for $\cos\alpha_i$ can be calculated starting from Fig. 1 along the values of the lattice constants (see Table 3). The components g_{ij} are obtained straightforwardly as $g_{11} = -3.6(1)\times10^{-5}$, $g_{22} = 10.7(9)\times10^{-5}$, $g_{33} = 27.0(4)\times10^{-5}$, and $g_{13} = -23.8(4)\times10^{-5}$. Its thermal dependence is beyond the resolution of the measurements.

In the literature and for most technological applications, it is convenient to express the rotation of the plane of polarization of the light per unit path in the medium, that is, as the rotatory power

$$\left(\frac{\varphi}{d}\right) = \frac{\pi G}{\lambda \bar{n}}. \tag{17}$$

This magnitude is shown in Table 3 for all the specimens at room temperature. The three-dimensional gyration surface, drawn with the Wintensor program [23], is illustrated in Fig. 6 at room temperature. Black areas designate the positive rotation, which is defined as a rotation of the plane of polarization clockwise by an observer whose eye the light is entering.

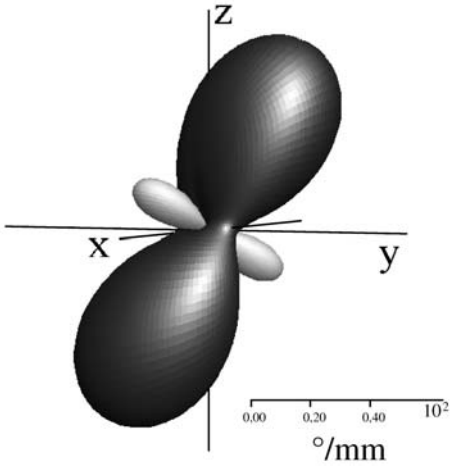

FIGURE 6 The gyration surface of LAP at room temperature. The values correspond to the optical rotatory power (°/mm). The *black* and *white areas* represent the positive and negative gyrations

4 Conclusions

The HAUP technique was applied successfully to determine the optical anisotropy of LAP as a function of temperature between 297 K and 359 K at a wavelength of 632.8 nm. A method to check the quality of the experimental results of the birefringence was applied, allowing us to find the birefringence for any propagation direction of the light beam theoretically from the experimental results. The thermal variation coefficient for a light beam along the y dielectric axis was found to be $-25.9\times10^{-6}\,\mathrm{K}^{-1}$, almost double that the coefficient for a light beam along the x and z dielectric axes, with $-16.9\times10^{-6}\,\mathrm{K}^{-1}$ and $-15\times10^{-6}\,\mathrm{K}^{-1}$ values, respectively. The gyration surface of LAP was also presented at room temperature and the tensor components in terms of rotatory power were found to be $\varrho_{11} = -6.6(3)°/\mathrm{mm}$, $\varrho_{22} = 19\,(2)°/\mathrm{mm}^{-1}$, $\varrho_{33} = 49.7(7)°/\mathrm{mm}$, and $\varrho_{13} = -43.7(8)°/\mathrm{mm}$ at a wavelength of 632 nm.

ACKNOWLEDGEMENTS This work has been supported by the Canary Islands Government (Project No. PI2001/093) and the FPU research grant from the Education, Culture and Sports Ministry of Spain awarded to J. H-C.

Appendix

We follow the method proposed by Kobayashiet al. [24] in order to get one of the principal refractive indices (n) for a given direction of the wave normal. The index n is expressed as

$$n = \frac{n_x n_z}{\left(n_x^2\cos^2\theta + n_z^2\sin^2\theta\right)^{1/2}}\,. \tag{A.1}$$

By substituting n_x by $n_z - \Delta n_y$ and dividing the numerator and denominator by n_z,

$$n = \frac{n_z\left(1-\Delta n_y/n_z\right)}{\left\{\left[1-2\left(\Delta n_y/n_z\right)+\left(\Delta n_y/n_z\right)^2\right]\cos^2\theta+\sin^2\theta\right\}^{1/2}}\,. \tag{A.2}$$

Upon introducing the variable x defined as $\Delta n_y/n_z$, we can write

$$n = n_z\,(1-x)\left(1-2x\cos^2\theta+x^2\cos^2\theta\right)^{-1/2}. \tag{A.3}$$

For a small birefringence, $|-2x\cos^2\theta + x^2\cos^2\theta| \ll 1$, and by using the approximation

$$(1+\alpha)^{-1/2} \sim 1 - 1/2\alpha\,, \tag{A.4}$$

(A.3) reduces to

$$n \approx n_z(1-x)\left(1+x\cos^2\theta - 1/2x^2\cos^2\theta\right). \tag{A.5}$$

Once again, $x \ll 1$ and so quadratic and higher orders are insignificant. Thus, the last equation takes the form

$$n \approx n_z(1-x\sin^2\theta) = n_z\cos^2\theta + n_x\sin^2\theta. \tag{A.6}$$

REFERENCES

1 K. Aoki, K. Nagamo, Y. Iitaka: Acta. Cryst. B **27**, 11 (1971)
2 D. Mucha, K. Stadnicka, W. Kaminsky, A.M. Glazer: J. Phys.: Condens. Matter **9** 10 829 (1997)
3 T. Ashai, M. Takahashi, J. Kobayashi: Acta Cryst. A **53**, 763 (1997)
4 W. Kaminsky: Rep. Prog. Phys. **63**, 1575 (2000)
5 D. Xu, M. Jiang, Z. Tan: Acta. Chim. Sin. **2**, 230 (1983)
6 D. Eimerl, S. Velsko, L. Davis, F. Wang, G. Loiacono, G. Kennedy: IEEE J. Quantum Electron. **QE-25**, 179 (1989)

7 A. Yokotani, T. Sasaki, K. Yoshida, S. Nakai: Appl. Phys. Lett. **55**, 2692 (1989)
8 G. Dhanaraj, M.R. Srinivasan, H.L. Bhat: J. Raman Spectrosc. **22**, 177 (1991)
9 G. Dhanaraj, M.R. Srinivasan, H.L. Bhat, H.S. Jayanna, S.V. Subramanyan: J. Appl. Phys. **72**, 3464 (1992)
10 B.A. Fuchs, C.K. Syn, S.P. Velsko: Appl. Opt. **28**, 4465 (1989)
11 A.M. Petrosyan, R.P. Sukiasyan, H.A. Karapetyan, S.S. Terzyan, R.S. Feigelson: J. Cryst. Growth **213**, 103 (2000)
12 W. Saenger, K.G. Wagner: Acta. Cryst. B **28**, 2237 (1972)
13 D. Eimerl, J. Marion, E.K. Graham, H.A. McKinstry, S. Haussühl: IEEE J. Quantum Electron. **QE-27**, 142 (1991)
14 J.F. Nye: *Physical Properties of Crystals*, 2nd edn. (Clarendon Press, Oxford 1985)
15 J. Kobayashi, Y. Uesu: J. Appl. Cryst.. **16**, 204 (1983)
16 J. Kobayashi, Y. Uesu, H. Takehara: J. Appl. Cryst. **16**, 212 (1983)
17 P. Gómez, C. Hernández: J. Opt. Soc. Am. B **15**, 1147 (1998)
18 J.R.L. Moxon, A.R. Renshaw: J. Phys.: Condens. Matter **2**, 6807 (1990)
19 J. Kobayashi, H. Kumoni, K. Saito: J. Appl. Cryst. **19**, 377 (1986)
20 D.A. Holmes: J. Opt. Soc. Am. **54**, 1115 (1964)
21 M. Born, E. Wolf: *Principles of Optics*, 7th edn. (Cambridge University Press, Cambridge 1999)
22 C. Hernández-Rodríguez, P. Gómez-Garrido, S. Veintemillas: J. Appl. Cryst. **33**, 938 (2000)
23 W. Kaminsky: Z. Kristallogr. Suppl. **12**, 183 (1997)
24 J. Kobayashi, K. Saito, N. Takahashi, I. Kamiya: Phys. Rev. B **48**, 10038 (1993)